ADVANCED MATERIALS

does not require the development of new capital equipment: filter (de-watering) presses are used in the clay industry to consolidate clay slurries, and isostatic presses are used to produce millions of spark plug insulators daily.

Received: August 17, 2000

[1] F. F. Lange, *J. Am. Ceram. Soc.* **1989**, *72*, 3.
[2] R. E. Mistler, D. J. Shanefield, R. B. Runk, "Tape Casting of Ceramics", in *Ceramic Processing Before Firing* (Eds: G. Y. Onoda, L. L. Hench), Wiley, New York **1978**, pp. 411–448.
[3] J. S. Reed, *Principles of Ceramic Processing*, 2nd ed., Wiley, New York **1995**, pp. 493–503.
[4] F. F. Lange, K. T. Miller, *Am. Ceram. Soc. Bull.* **1987**, *66*, 1498.
[5] J. A. Mangels, *Ceram. Eng. Sci.* **1982**, *3*, 529.
[6] A. C. Young, O. O. Omatete, M. A. Janney, P. A. Menchhofer, *J. Am. Ceram. Soc.* **1991**, *74*, 612.
[7] T. J. Graule, F. H. Baader, L. J. Gauckler, *Ceram. Forum Int./Ber. DKG* **1994**, *71*, 317.
[8] G. V. Franks, B. V. Velamakanni, F. F. Lange, *J. Am. Ceram. Soc.* **1995**, *78*, 1324.
[9] G. W. Scherer, *J. Am. Ceram. Soc.* **1990**, *73*, 3.
[10] V. K. Pujari, *Am. Ceram. Soc. Bull.* **1995**, *74*, 86.
[11] G. V. Franks, F. F. Lange, *J. Am. Ceram. Soc.* **1996**, *79*, 3161.
[12] J. C. Chang, F. F. Lange, D. S. Pearson, J. P. Pollinger, *J. Am. Ceram. Soc.* **1994**, *77*, 1357.
[13] R. G. Horn, *J. Am. Ceram. Soc.* **1990**, *73*, 1117.
[14] D. C. C. Lam, K. Kusakari, *J. Mater. Sci.* **1995**, *30*, 5495.

One-Dimensional Quantum Confinement in Electrodeposited PbS Nanocrystalline Semiconductors**

By *Karunakar K. Nanda* and *Surendra N. Sahu**

Nanocrystalline semiconductor particles with a size comparable to the Bohr exciton radius exhibit quantum-confinement effects where the continuum of energy levels are broken down into discrete states with an energy level spacing $>kT$ and this results in the widening of the bandgap. Within a simple effective-mass approximation, the confined gap E_{cg} is given by[1]

$$E_{cg} = E_g + \frac{\eta^2\pi^2}{2}\left[\frac{1}{w_x^2}+\frac{1}{w_y^2}+\frac{1}{w_z^2}\right]\left[\frac{1}{m_c^*}+\frac{1}{m_v^*}\right] \quad (1)$$

where m_c^* and m_v^* are the conduction and valence band effective masses, respectively. The other parameters w_x, w_y, and w_z are the dimensions of a three-dimensional (3D) box. If $w_x \ll w_y$ & w_z, then the energy levels will be controlled by w_x. This implies that the optical properties of a non-spherical nanocrystal are controlled by the lowest dimension of the nanocrystal and the carriers are confined in one dimension only. Similar one-dimensional confinement has already been observed for PbS semiconductors.[2] In this letter, we focus on the synthesis of the PbS semiconductor nanocrystalline films by an electrochemical route and study the size quantization effect. Optical absorption and the atomic force microscopy (AFM) images provide evidence for the one-dimensional quantum confinement within the PbS nanocrystals. A classical interpretation is provided to predict the shape of the nanocrystallites and the X-ray characterization of the materials is discussed.

PbS nanocrystalline films on indium tin oxide (ITO) glass and titanium (Ti) were grown by a cathodic electrodeposition technique from a solution containing $Pb(NO_3)_2$ (0.02 M) and $Na_2S_2O_3$ (0.1 M) with pH 0.62. The thiosulfate solution (< pH 2.3) dissociates according to the reaction:[3]

$$S_2O_3^{2-} \longrightarrow S + SO_3^{2-}$$

and the overall cathodic reaction is given as

$$Pb^{2+} + S_2O_3^{2-} + 2e^- \longrightarrow PbS + SO_3^{2-}$$

resulting in the formation of PbS at the cathode and colloidal sulfur in the bulk solution. The cathodic process results in the chemisorption of Pb^{2+} followed by reduction and surface diffusion. Further, chemical reaction with $S_2O_3^{2-}$ leads to the formation of PbS nanoparticles. The crystallite sizes were controlled by varying the electrolysis current and the temperature of the solution. Increasing the current yields smaller particles, whereas higher temperatures yield larger particles. The crystallite size can also be controlled by adjusting the deposition time and thus the thickness of the deposited films. Increasing the thickness yields larger crystallites as is the case with chemically deposited CdS.[4] Hence, in order to achieve a narrow size distribution, the thickness of the sample should be small. Typical values of the electrolysis current density and temperature used to obtain nanocrystalline PbS with a thickness of 60 nm (to be discussed later) are 2 mA/cm^2 and 280 K, respectively.

As there are a small number of atoms in a cluster, inclusion of any impurities may have dramatic effects on the optical properties of the films.[5] It is therefore essential to ascertain the chemical purity of the deposit. Proton-induced X-ray emission (PIXE) analysis using an H^+ beam of 2.98 MeV from a 3 MV pelletron accelerator indicated the absence of any impurities, even at the ppm level. Rutherford backscattering spectroscopy (RBS) analysis was carried out at a scattering angle of 155° using a 3.049 MeV He^{2+} beam and the RBS spectrum is shown in Figure 1. The presence of Pb and S along with oxygen and the substrate (Ti) contribution are identified. The composition (Pb to S ratio) and thickness were estimated to be 0.9 and 60 nm, respectively, obtained by simulating the raw data as shown in Figure 1. Note that the oxygen yield, even at a resonance energy of 3.049 MeV, is small and suggests that the oxygen originates from ITO alone.

The X-ray diffraction (XRD) pattern of the PbS sample is shown in Figure 2. The analysis reveals a cubic phase with prominent planes (200), (220), and (311) (not shown here). The average size of the nanocrystallites can be determined

[*] Dr. S. N. Sahu, Dr. K. K. Nanda
Institute of Physics
Sachivalaya Marg
Bhubaneswar-751005 (India)
E-mail: sahu@iopb.res.in

[**] Helpful discussions with Prof. V. S. Ramamurthy and Prof. S. N. Behera are gratefully acknowledged. The AFM measurements were carried out at TIFR, Mumbai (India) and the help of Dr. S. Tripathi is gratefully acknowledged.

  0935-9648/01/0402-0280 $ 17.50+.50/0

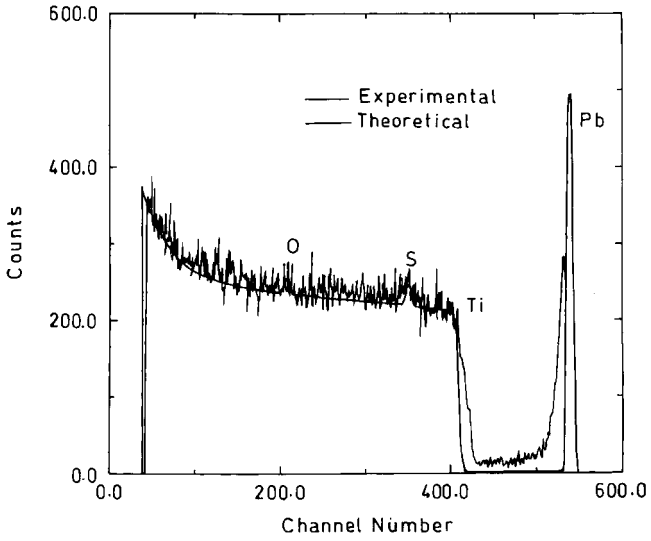

Fig. 1. Rutherford backscattering spectrum of the PbS sample. The incident beam is 3.049 MeV He^{2+}. The solid line is the theoretical fit to the data. For this sample the Pb to S ratio is found to be 0.9.

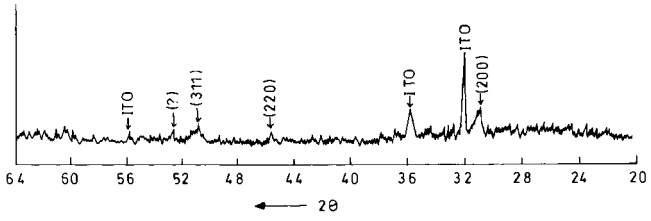

Fig. 2. XRD patterns of the PbS sample. The crystalline size estimated from the line broadening is 17.5 nm.

from the line broadening using Scherrer's equation[6] $D = \kappa\lambda/\beta\cos\theta$, where β is the half width of the diffraction peak, λ is the X-ray wavelength, and κ is a geometrical factor taken to be 1. The particle diameter determined in this way from the peak (200) is 17.5 nm. Furthermore, the XRD patterns do not indicate sulfur as a separate phase implying that the excess sulfur (estimated from RBS) has become an interstitial component of the lattice. For large size particles, obtained by varying the electrolysis current density and temperature, well-defined (200), (220), and (311) peaks are observed (the details will be published elsewhere). The formation of the nanocrystalline PbS has also been confirmed from Raman scattering measurements.[7]

The sizes of the nanocrystallites were also determined by AFM studies (Fig. 3). The detail of the imaging procedure is described in the literature.[4] The crystallite size is estimated to be 20 nm, which is very close to that obtained from X-ray line broadening.

PbS is a low bandgap semiconductor whose bulk bandgap is 0.41 eV and the Bohr exciton radius is 20 nm.[8] As the particle size in our case is of the order of 20 nm, we would expect quantum size effects in the optical absorption spectrum. Figure 4 shows the optical absorption spectrum of the PbS sample prepared on ITO glass. Note that the exciton peak appears at 2.63 eV (470 nm) in good agreement with earlier

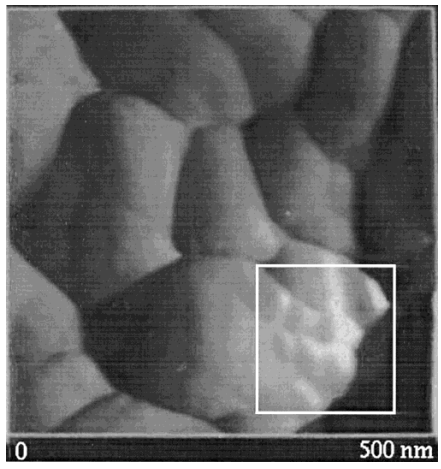

Fig. 3. AFM image of PbS sample. From the region specified by a square, the average crystalline size is estimated to be 20 nm.

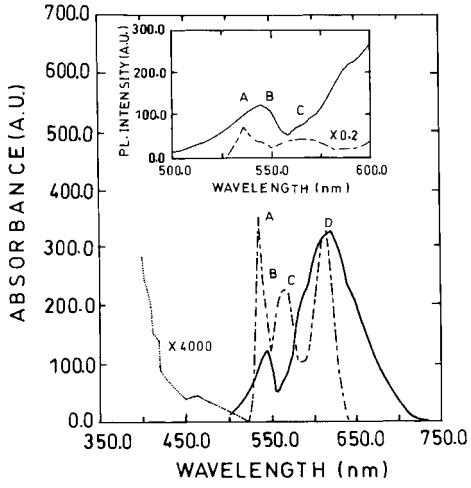

Fig. 4. Optical absorption spectrum (thin line), photoluminescence spectrum at 150 K (thick line), and 15 K (broken line) of PbS nanocrystallites with an excitonic peak at 2.63 eV as marked by an arrow. Inset: An expanded view of the photoluminescence spectra.

reported results.[6] This peak corresponds to the transition from the highest occupied molecular orbital (HOMO) in the valence band to the lowest unoccupied molecular orbital (LUMO) in the conduction band. Some important observations are summarized below.

- In narrow gap semiconductors, the large exciton radius and the strong screening can give a small exciton binding energy which results in the absence of excitonic structure. So far excitonic structures have been observed for large bandgap semiconductors, e.g., CdS, ZnS, and GaN, only at low temperature. However, in nanoparticles, the exciton peak is observed even at room temperature due to enhancement of the exciton oscillator strength because of the strong overlap of the wavefunctions of the confined electron and hole which diverges as $(a_B/r)^3$.[9]
- From ab-initio calculations,[6] it is predicted that the lowest excitation energy of a single PbS molecule is 2.51 eV which is very close to that obtained in our nanocrystalline PbS sample. However, if we plot the square of the absorp-

  0935-9648/01/0402-0281 $ 17.50+.50/0

ADVANCED MATERIALS

tion vs. energy, we obtain a value of E_g of 2.4 eV. In the ab-initio calculations the bandgap is evaluated by considering the lattice parameter of nanoparticles to be the same as that for the bulk material (0.5936 nm). However, the lattice parameter in our PbS sample is 0.58546 nm for which a larger bandgap is expected. Interestingly, a bandgap as large as 5.2 eV has also been reported.[10]

- Normally, a tail due to off-stoichiometry and sub-bandgap absorption due to a separate phase[11] can be expected in the long wavelength regime of the absorption spectrum. Note that this feature in the absorption spectrum is not seen in our case. This implies that the absorption spectrum is solely due to PbS though there is excess sulfur as interstitial in the sample in good agreement with XRD result. However, the effect of off-stoichiometry and the presence of oxygen could be reflected in the X-ray photoemission (XPS) studies which are in progress.

The photoluminescence spectra of the nanocrystalline PbS sample at 150 and 15 K are also shown in Figure 4 along with the optical absorption spectrum. Note that each spectrum consists of four bands in the wavelength range 500 to 800 nm (marked a–d) which are clearly resolved at low temperature. The position of the first three bands (a–c) are almost independent of temperature in contrast to the d band which shifts to higher energy by 10 meV when the temperature is lowered from 150 to 15 K. However, the intensity increases and the full width at half maximum (FWHM) decreases as the temperature is lowered which can be ascribed to the insignificant contribution of phonons to the luminescence.

It can be noted from Figure 4 that the first emission band (a) overlaps with the absorption threshold which can be assigned to a recombination of free excitons. The exciton binding energy is the difference[12] in energy (δE) between the first maximum in the absorption spectrum and the highest energy luminescence band arising due to Coulomb electron–hole interaction given by:[13]

$$\delta E = \frac{1.786e^2}{\varepsilon r} \tag{2}$$

where e, ε, and r are the electronic charge, dielectric constant, and the radius of the nanoparticle, repectively. In our PbS case, the exciton binding energy is found to be ~300 meV which corresponds to a size of ~1.8 nm. Furthermore, the second band (b) is located at a lower energy, about 25 meV lower than the "a" band, and can be assigned to a recombination of bound excitons whose energy is always less than the free exciton energy. Note that the energy of band c is less than that of the "b" band by 100 meV and is therefore ascribed to donor–acceptor recombination (as is the case with GaN[14]) and the "d" band is located at the lowest energy side of the spectrum and can be assigned to a surface-related band as described elsewhere.[10] However, experiments are in progress to identify these peaks unambiguously. To the best of our knowledge, this is the first report which identifies the free and bound excitons in PbS nanocrystalline samples.

As the crystallite size obtained from AFM and that estimated from the exciton binding energy do not match, the average size of the PbS nanocrystallites were also estimated from the blue shift. A hyperbolic band model[6] has been suggested to explain the change of the energy gap as a function of particle size with the assumption that the nanoparticles are spherical. The equation derived for the change in bandgap ΔE according to this model is:

$$\Delta E = [E_g{}^2 + 2\eta E_g(\pi/r)^2/m^*]^{1/2} - E_g \tag{3}$$

where E_g is the bandgap for the bulk semiconductor, r the particle radius, and m^* the effective mass of electron. Once, the bandgap is known, the corresponding particle size can easily be estimated using the above equation. For our nanocrystalline PbS sample, the bandgap is 2.63 eV (470 nm). Taking $m^*/m_e = 0.085$, where m_e is the free electron mass and E_g = 0.41 eV for bulk PbS, the particle diameter was found to be ~2.0 nm which is very close to that obtained from the exciton binding energy by using Equation 2. On the other hand, the AFM analysis (Fig. 3) shows a lateral dimension of 20 nm. This discrepancy is ascribed to a pancake geometry of the nanocrystallites with a diameter of 20 nm and a height of 2.0 nm. A similar geometry with a diameter of 12 nm (AFM) and a height of 5 nm (from optical absorption) has also been observed in case of chemically deposited CdS samples.[4] As the diameter-to-height ratio is large, it can be concluded that the charge carriers are confined in one dimension only. In the case of electrodeposition with constant current one would expect a local variation of current density at the cathode which would result in 2D growth.[15] Furthermore, AFM measures the lateral dimension of the crystallites on the top layer, whereas optical absorption determines the average height of the crystallites. Therefore, such a high value of the diameter-to-height ratio is obtained in the case of PbS (20:2) in good agreement with the predicted shape of the metallic clusters.[16–19]

Classical Interpretation of Non-Spherical Geometry: Like the nucleons in the nucleus, the atoms in the nanoparticles are held together by short range attractive forces. These forces reduces the mass of the particle below that of its constituents by an amount proportional to the number of atoms (N). Since the volume of the particles is proportional to N, the volume binding energy is given by

$$E_v = a_v N \tag{4}$$

where a_v is a proportionality constant and the subscript v is for volume.

Since the nanoparticles are of finite size, some of their constituent atoms are on the surface and the proportion of surface atoms increases as the particle size decreases. If the geometry of the particle is considered to be spherical with a radius r, then the surface to volume ratio (A) can be given as

$$A = \frac{4\pi r^2}{4\pi r^3/3} = \frac{3}{r} \tag{5}$$

  0935-9648/01/0402-0282 $ 17.50+.50/0

When r is of the order of few nanometers, the particles are named nanoparticles and the surface effects of the particle can not be neglected. The atoms on the surface are less tightly bound than those in the interior. Thus, in case of small particles the volume binding energy is reduced by an amount proportional to the surface of the particle and is proportional to r^2 or $N^{2/3}$ and is given by

$$E_s = a_s N^{2/3} \tag{6}$$

where a_s is the proportionality constant and s denotes the surface.

Combining Equation 5 and Equation 6, one obtains the binding energy per atom as

$$\frac{E_b}{N} = a_v - \frac{a_s}{N^{1/3}} = a_v - \frac{a_s}{r} \tag{7}$$

It is noted that as the particle size decreases the binding energy per atom decreases and hence the spherical nature can not be retained. In contrast, Wang et al.[6] have found that the size determined from optical absorption for PbS nanoparticles agrees well with transmission electron microscope (TEM) and XRD results implying a spherical nature which is expected as the particles are polymer capped.

Diffractogram of "Pancake-like" Particles: It has been shown[20] that the diffractogram of an ellipsoid will be different from that of a sphere with equal volume and depends on the axes of the ellipsoid. It is also known that as the half width is large in the case of a sphere compared to an ellipsoid of the same volume, the size estimated from the XRD spectra using Scherrer's equation is expected to be large in the case of the ellipsoid. As the pancake shape can be approximated as an ellipsoid, the diffractogram is expected to be similar. The volume of a pancake of diameter 20 nm and height 2 nm is the same as the volume of a sphere with diameter ~11 nm which is smaller than the value obtained from the XRD pattern (17.5 nm) as expected for a pancake structure.

In summary, lead sulfide semiconducting nanoparticulate thin films having pancake-like geometry have been synthesized by an electrochemical route. Due to the non-sphericity of the crystallites, the optical properties of the nanoparticles are controlled by the lowest dimension of the particles—a consequence of one-dimensional quantum confinement. Optical absorption at 300 K and photoluminescence at lower temperatures reveal that the bandgap of the nanoparticles does not change with temperature in contrast to the reported temperature dependence in bulk lead sulfide where the bandgap shifts to lower energy as the temperature decreases. We also report the feature of free and bound excitons in lead sulfide nanoparticles, which become more prominent as the temperature is lowered.

Received: April 10, 2000
Final version: August 4, 2000

[1] R. T. Collins, F. M. Fauchet, M. A. Tischler, *Phys. Today* **1997**, *47*, 24.
[2] X. K. Zhao, L. D. McCormick, *Appl. Phys. Lett.* **1992**, *61*, 849.
[3] E. Fatas, R. Duo, P. Herrasti, F. Arjona, E. Garcia-Camarero, *J. Electrochem. Soc.* **1984**, *131*, 2243.
[4] K. K. Nanda, S. N. Sarangi, S. Mohanty, S. N. Sahu, *Thin Solid Films* **1998**, *322*, 21.
[5] R. N. Bhargava, D. Gallagher, X. Hong, A. Nurmikko, *Phys. Rev. Lett.* **1994**, *72*, 416.
[6] Y. Wang, A. Suna, W. Mahler, R. Kawoski, *J. Chem. Phys.* **1987**, *87*, 7315.
[7] K. K. Nanda, S. N. Sahu, R. K. Soni, S. Tripathy, *Phys. Rev. B* **1998**, *58*, 15 408.
[8] T. D. Krauss, F. W. Wise, D. B. Tanner, *Phys. Rev. Lett.* **1996**, *76*, 1376.
[9] Y. Kayanuma, *Phys. Rev. B* **1988**, *38*, 9797.
[10] R. Thielsch, T. Bohme, R. Reiche, D. Schlafer, H.-D. Bauer, H. Bottcher, *Nanostruct. Mater.* **1998**, *10*, 131.
[11] N. Kavcar, *Sol. Energy Mater. Sol. Cells* **1998**, *52*, 183.
[12] J. von Behren, T. van Buuren, M. Zacharias, E. H. Chimowitz, P. M. Fauchet, *Solid State Commun.* **1998**, *105*, 317.
[13] N. R. Kulish, V. P. Kunets, M. P. Lisitsa, *Superlattices Microstruct.* **1997**, *22*, 341.
[14] J. Menniger, U. Jahn, O. Brandt, H. Yang, K. Ploog, *Phys. Rev. B* **1996**, *53*, 1881.
[15] R. K. Pandey, S. N. Sahu, S. C. Chandra, *Handbook of Semiconductor Electrodeposition*, Marcel Dekker, New York **1996**, Ch. 3.
[16] C. J. Coombes, *J. Phys. F* **1972**, *2*, 441.
[17] R. Kofman, P. Cheyssac, R. Garrigos, Y. Lereah, G. Feutscher, *Z. Phys. D* **1991**, *20*, 267.
[18] C. H. De Villeneuve, L. Porte, L. Bardotti, B. Cabaud, A. Hoareau, M. Treilleux, *Microsc. Microanal. Microstruct.* **1993**, *4*, 471.
[19] I. Ostadal, J. Myslivecek, P. Sobtik, *Vacuum* **1998**, *50*, 179.
[20] A. Guinier, *X-Ray Diffraction in Crystals, Imperfect Crystals, and Amorphous Bodies*, Dover, New York **1994**, 319.

Simple Synthesis of MoS_2 and WS_2 Nanotubes

By *Manashi Nath*, *Achutharao Govindaraj*, and *C. N. R. Rao**

Carbon nanotubes constitute an important class of materials with several potential applications. By analogy to the fullerenes and carbon nanotubes, Tenne et al.[1–3] suggested that layered metal dichalcogenides could form similar fullerene-related structures. Nanotubes of MoS_2 have indeed been produced and characterized by Tenne and co-workers.[4] Their method of preparation of the MoS_2 nanotubes employs the gas-phase reaction between MoO_3 and H_2S in the presence of argon. The procedure involves heating solid MoO_3 in a stream of forming gas (95 % N_2 + 5 % H_2) to reduce the oxide to some extent, followed by the reaction of the oxide with a stream of H_2S mixed with the forming gas. The product contained nanotubes of MoS_2 along with polyhedral particles. The mechanism of forming MoS_2 has been suspected to involve a trisulfide intermediate.[3] Based on the literature[5,6] and our own experience with the reaction between MoO_3 and H_2S, there seemed little doubt that the reaction of MoO_3 with H_2S gives amorphous MoS_3 as the product. The MoS_2 nanotubes are therefore to be expected to be formed following the decomposition of MoS_3. We therefore decided to examine the transformation of MoS_3 at high temperatures in a hydrogen

[*] Prof. C. N. R. Rao,[+] Dr. A. Govindaraj, M. Nath
CSIR Centre for Excellence in Chemistry & Chemistry and Physics of Materials Unit
Jawaharlal Nehru Centre for Advanced Scientific Research
Jakkur P.O., Bangalore 560 064 (India)
E-mail: cnrrao@jncasr.ac.in
[+] Second address: Solid State and Structural Chemistry Unit, Indian Institute of Science, Bangalore 560 012, India.

  0935-9648/01/0402-0283 $ 17.50+.50/0